ELSEVIER

Polymer 41 (2000) 4513–4521

polymer

Morphology and fracture toughness of poly(ether sulfone)-blended polycyanurates

Jer-Yuan Chang[a], Jin-Long Hong[b,*]

[a]*Department of Chemical Engineering, Yung-Ta Institute of Technology and Commerce, Ping-Tung, Taiwan, ROC*
[b]*Institute of Materials Science and Engineering, National Sun Yat-Sen University, Kaohsiung, Taiwan, ROC*

Received 19 January 1999; received in revised form 2 July 1999; accepted 11 August 1999

Abstract

Polycyanurate derived from bisphenol A dicyanate (BPADCy) is brittle in nature; therefore, different amounts of hydroxyl- or cyanate-terminated poly(ether sulfone) (as HPES or CPES) was mixed and heated with BPADCy to obtain a thermoplastic-blended polycyanurate. Morphology of this thermoplastic-blended polycyanurates was investigated by SEM, and their fracture toughness was evaluated by the propagation of the deformation zone after immersion of the sample film in methylene chloride. The results suggest that polycyanurate blended with 50 wt% of HPES (or CPES) has higher fracture toughness than sample toughened with 10 wt% of HPES (or CPES). In addition, polycyanurates blended with CPES usually have higher fracture toughness than those blended with same amounts of HPES. These results can be qualitatively correlated with the morphology difference observed from the SEM study.

Keywords: Polycyanurates; Poly(ether sulfone); Morphology

1. Introduction

Rubber particles and thermoplastics have been used for a long time to improve the toughness of thermosetting resins [1]. A general description for the toughened thermosetting system is the two-phase morphology formed during curing at elevated temperatures. A variety of different morphologies, and therefore mechanical properties can be obtained from rubber-toughened epoxy resins [2–6]. The volume fraction, domain size, and the number of particles of phase-separated rubber, factors that can be varied by composition, curing temperature, and gelation time, are all crucial to the final mechanical properties of the cured products.

Polycyanurate resins prepared from the curing reactions of aromatic dicyanates [7–9] had gained increasing attention due to their low dielectric constants, high thermal stability, high glass transition temperature (250 ~ 280°C), low water/moisture sorption and excellent processability. Due to the brittle nature of the polycyanurate resins, several thermoplastics [10–14] such as polycarbonate, poly(ethylene terephthalate), polysulfone and poly(ether imide) had been previously used to toughen different polycyanurates. Most referred studies here had concentrated on the variations of morphology and composition. Among them, Woo et al. [13] described the structure variation from a thermosetting continuity to a co-continuity of both components in a poly(aryl sulfone)/bisphenol-E dicyanate (PS/BPEDCy) system when volume % of PS changes. Dynamic mechanical data of these binary blends [14] were further fitted with a modified Takayangi model based on the structure changes observed by optical and electron microscopy.

Previously, we had synthesized hydroxyl- or cyanate-terminated poly(ether sulfone) (as HPES and CPES, respectively), and mixed them with bisphenol A dicyanate (BPADCy) and heated to prepare thermoplastic-blended polycyanurates [15]. Through various reaction conditions including use of different thermoplastic components (HPES or CPES), composition, or catalyst for polycyclotrimerization, the cured products have a two-phase morphology of varied structures with different interfacial adhesion and particle sizes. These structures should consequently influence the mechanical properties of the cured products, and correlation between their fracture toughness and morphological parameters can be thus evaluated.

In this study, thermal properties and fracture toughness (G) of the toughened polycyanurates were surveyed by plane stress approach for an infinitely large cracked plate [16,17]. The method to evaluate the fracture toughness involves immersion of the sample film with pre-formed crack and measurement of the deformation zone at different time period. The related equation is $G = \pi\sigma^2 a/E$ (where a is

* Corresponding author. Tel.: +886-7-5252000; fax: +886-7-5254099l.
E-mail address: jlhong@mail.nsysu.edu.tw (J.-L. Hong).

0032-3861/00/$ - see front matter
PII: S0032-3861(99)00616-3

Table 1
Sample code and weight percentage of the starting mixture of HPES (or CPES) and BPADCy

Sample code	Component 1 (weight percentage, %)	Component 2 (weight percentage, %)	Catalyst
BH-10	BPADCy (90)	HPES (10)	None
BH-50	BPADCy (50)	HPES (50)	None
BC-10	BPADCy (10)	CPES (90)	None
BC-50	BPADCy (50)	CPES (50)	None
BH-10C1	BPADCy (10)	HPES (90)	Yes[a]
BH-50C1	BPADCy (50)	HPES (50)	Yes[a]

[a] One wt% of catalyst system (NP/Co(acac)$_2$) was added.

the flaw size, σ is the stress level and E is the elastic modulus at fracture). An optical microscope (OM) was used to observe the process of solvent-induced fracture. The mechanism of the solvent-induced fracture was therefore proposed. In addition, differential scanning calorimetry (DSC), scanning electron microscopy (SEM), and transmission electron microscopy (TEM) were applied to resolve thermal properties and fracture surface of the thermoplastic-blended polycyanurates.

2. Experimental

2.1. Materials

HPES and CPES were prepared according to procedures described previously [18,19]. Molecular weights of HPES ($M_n = 22,000$, $M_w = 40,900$, MWD = 1.86) and CPES ($M_n = 22,000$, $M_w = 41,360$, PD = 1.88) were determined from gel permeation chromatography with THF as eluent and polystyrene as standard. The densities of HPES, CPES and BPADCy were measured by the density gradient method. To a mixture of the corresponding sample in small amounts of distilled water, 50 wt% aq. NaOH solution was added drop by drop until the moment the sample was floated on the solution surface. The density was assumed to be equal to that of the mixture solution, which can be calculated by the known amounts of the added NaOH.

Mixtures of HPES (or CPES) and BPADCy were prepared by melt-mixing method, primarily used by Brown and Yang [16]. BPADCy was heated to about 130°C and HPES (or CPES) in a fine powder form was added slowly with continuous stirring. Complete mixing was judged by the transparency of the mixture. The catalyst system was prepared by blending *n*-nonylphenol and cobalt acetylacetone (NP/Co(acac)$_2$) at a weight ratio of 100 to 8. For the catalyzed system, catalysts were added at the later stage of mixing. The resulting mixture was then vacuum dried at 130°C to remove air/vapor bubbles. The resulting homogeneous liquid mixtures were dropped between two parallel strips of glass fibers (100 μm thick) fixed on glass slides in a longitudinal direction. Then a glass rod was moved along the longitudinal direction with its two ends striding over the glass fiber. A thin film of 100 μm thick was thus formed and subjected to further isothermal curing at 200°C for 90 min, and 280°C for 30 min. The resulting films were further inspected by POM and SEM.

2.2. Instrumentation

A Dupont DSC 910 cell connected to a DuPont 9900 data station was used to detect the thermal properties of the cured products. The cured products were prepared by thorough mixing of the two components at 130°C before the subsequent curing at 200°C for 90 min and 280°C for 30 min. Cured products of approximately 5 mg were sealed in a hermetic aluminum pan and heated in the temperature ranges of 30–450°C. Calibration of the calorimeter was conducted for each heating rate using an indium standard.

A Nikon Optical Microscope equipped with a THMS 600 hot stage, a Linkam TMS controller and a SONY video recorder was used for measurement of the flaw size of the cured products. A thin film of the cured product with a thickness of 100 μm was prepared for the flaw measurement. Since line defects were easily nucleated at the sample edges if films on the glass slides were directly immersed in methylene chloride, small holes with a diameter of 100 μm was introduced in the central region of the film with a razor blade to control the nucleation rate. After immersion in methylene chloride for different time periods the thin films were then withdrawn and dried in air before inspection by POM. Deformation zone lengths developed at different sample regions and time periods were measured and recorded. For each measurement, only straight-line deformation was considered since formation of a loop in the later stage (cf. Fig. 9) was highly possible. Deformation zone length at 1 min (the time at which a steady flaw growth started) after initiation was recorded and the average value of five deformation zone lengths was taken as the flaw size, a. The stress level, σ, was calculated from a rule of mixture, $\sigma = \sigma_1 v_1 + \sigma_2 v_2$ (where, the subscript 1 represents the cured BPADCy and 2 stands for the second poly(ehter sulfone) component, v_i refers to the volume fraction of component i). Analogously, the elastic modulus at fracture, E, was evaluated from $E = E_1 v_1 + E_2 v_2$. Here, σ and E values of the pure poly(ether sulfone) and cured BPADCy components were obtained from the literature [20,21]. The corresponding fracture toughness, G, was then calculated from $G = \pi\sigma^2 a/E$.

The morphology of the cured resin was examined by a Jeol JSM-6400 scanning electron microscope operated at a 20 kV accelerating voltage. Thermoplastics-blended samples were first fractures in liquid nitrogen, then, the fracture surface was coated with gold by vapor deposition using a Polaron SC502 vacuum sputter coater.

A Jeol JEM-100S transmission electron microscope was employed to examine the interfaces between the second

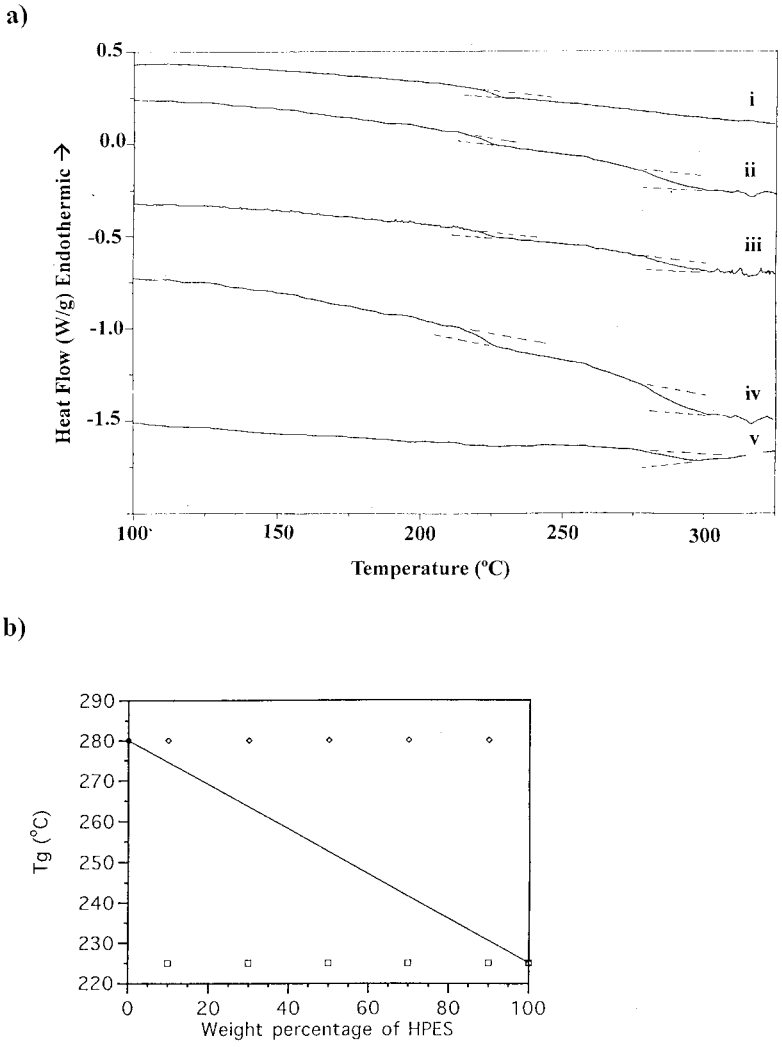

Fig. 1. (a) DSC thermograms of (i) pure HPES, and the cured (ii) BH-10, (iii) BH-30, (iv) BH-50, and (v) BPADCy (Heating rate = 10°C/min). (b) Glass transition temperatures versus compositions for the cured BH system.

phase and the matrix. The specimen was embedded in a cured epoxy resin, sectioned to 30–45 nm thick by ultromicrotome of Reichert Ultracut E, and then stained with 1 wt% aqueous solution of ruthenium tetroxide.

2.3. Sample code

The sample code for the starting liquid blends is designated as BH (or BC)-X shown in Table 1. The first capital B stands for BPADCy, the second H (or C) for HPES (or CPES), and the number X after the dash is the weight percentage of the HPES (or CPES) applied in the starting mixture. In a catalyzed system, an additional C1 is used to represent that 1 wt% of the catalyst system was used in this blend.

3. Results and discussion

Primary characterizations of the cured products were concentrated on the thermal properties. Selected DSC thermograms of the cured BPADCY/HPES (as BH) were given in Fig. 1a. Here, all DSC thermograms showed the presence of two T_gs, indicating a two-phase morphology for all samples. The pure components, HPES and the cured BPADCy, have their respective T_gs appeared at around 225 (curve i) and 280°C (curve v); with the inclusion of the second component, the cured products in the BH system all have their two T_gs at ~225 and 280°C. This result can be illustrated by the T_g-composition curve shown in Fig. 1b, in which products ranging from the compositions of 10–90 wt% exhibit the same T_g values. Suggestively, the constant T_gs versus composition implies little miscibility between HPES and the polycyanurate network derived from BPADCy.

DSC thermograms of the cured BPADCy/CPES (as BC) sample were shown in Fig. 2a. The presence of two T_gs in all cases also suggests a two-phase morphology in samples of different compositions; however, in contrast to the cured BH

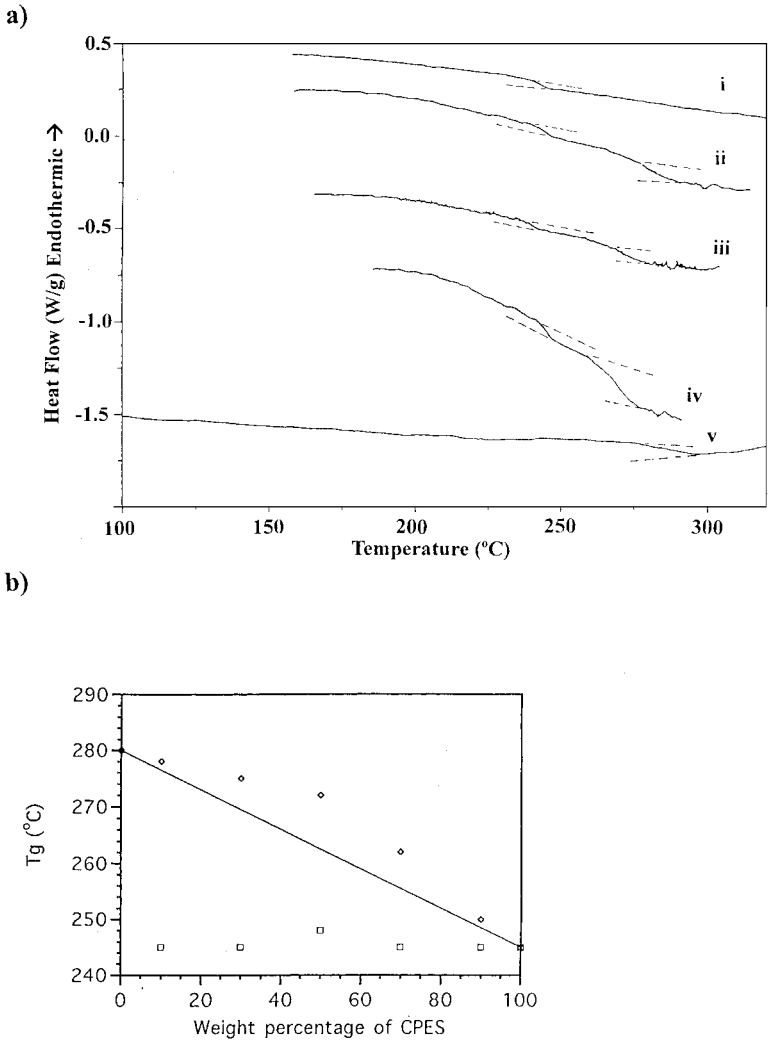

Fig. 2. (a) DSC thermograms of the cured (i) CPES, (ii) BC-10, (iii) BC-30, (iv) BC-50, and (v) BPADCy (Heating rate = 10°C/min). (b) Glass transition temperatures versus compositions for the cured BC system.

system described above, variations of the high-temperature T_gs with compositions were observed in this system. The cured CPES has its T_g (curve i) located at approximately the same position with the low-temperature T_gs of other cured products in the BC system; in contrast, the high-temperature T_gs originated from the BPADCy-derived component (as BPADCy-rich phase or domain) increase with the decreasing CPES content (compare curves iv with ii or iii). This particular feature can be best demonstrated by the T_g-composition curve shown in Fig. 2b, in which the non-linear dependence of the high-temperature T_g versus composition is clearly illustrated. At this moment, we can suggest that there are certain degrees of mutual miscibility between the cured CPES and BPADCy components in the BC system. The T_g reduction of the BPADCy-rich phase with the increasing CPES content may indicate the incorporation of the CPES-component into the BPADCy-rich network through the inter-reactions of the -OCN groups in the CPES and BPADCy. On the contrary, the intact low-temperature T_g with composition suggests the absence of the cured BPADCy in the CPES-rich phase. Further morphological study in this manuscript will support this point but before that, the cause for this particular feature should be discussed. High molecular weight ($M_n = 22,000$) CPES is supposed to have a lower curing rate than the cure of BPADCy ($M_n = 278$) in considering the low concentration of the -OCN terminals in CPES. During the cure of the BPADCy/CPES mixture, formation of the BPADCy-rich phase should be the predominant process initially in view of the higher reaction rate of BPADCy as compared with cure of CPES. The preferable formation of BPADCy-rich domain may efficiently reject the CPES chains due to the concurrent free energy difference accompanied by the cure. However, at a later stage after most of the uncured CPES had been removed form the cured BPADCy domains, polycyclotrimerization of CPES became possible since the produced *s*-triazine ring would catalyze this less potent reaction [19]. The residual CPES chains remaining in the

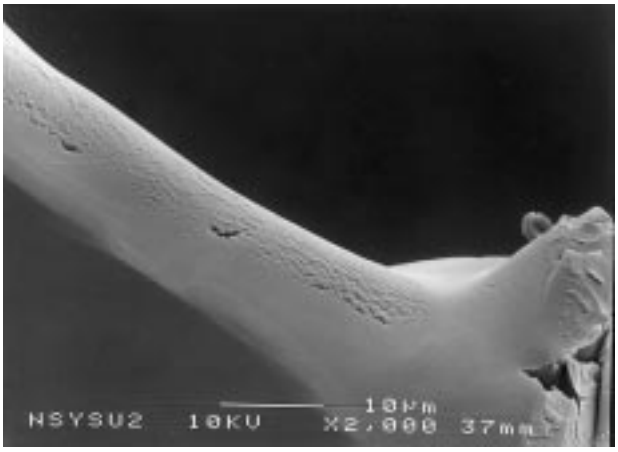

Fig. 3. Fractograph of the cured BPADCy. The specimen was cured at 200°C for 90 min, and then post-cured at 280°C for 30 min.

BPADCy-rich domain would be trapped in the BPADCy-rich domains and cure at a later stage. The CPES chains ejected at the early stage formed the other phase which is unaffected by the cured BPADCy.

Fracture surfaces of the selected samples were examined by SEM to evaluate the morphological difference due to component, composition, and curing conditions applied in the preparation step. Our primary test was the neat, cured BPADCy. With no inclusion of any second component, the fracture surface of pure BPADCy (Fig. 3) was quite smooth, indicating the brittle nature of the cured BPADCy. In contrast to the single-phase morphology of the cured BPADCy, the fracture surface of the cured BH-10 shows the discrete–continuous morphology with the matrix phase continuously interconnected and the other as discrete spherical particles hidden inside the continuous matrix phase (Fig. 4). The particle phase can be removed by continuous extraction with methylene chloride, indicating that this phase is enriched in HPES. The fractograph of the fractured surface suggests that cracks propagate along the particle-matrix boundary, resulting in obvious cavitation and plastic deformation on the matrix side of the interface.

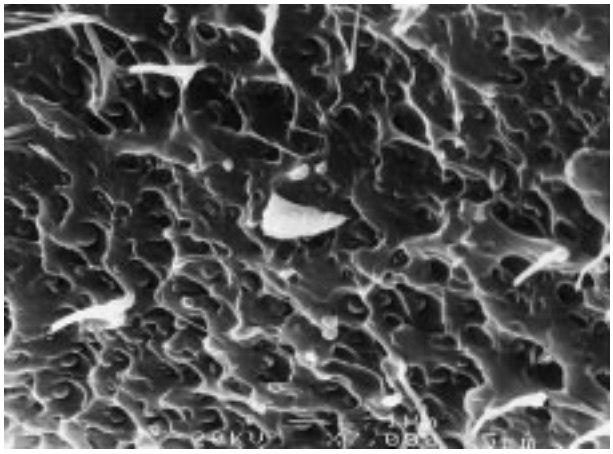

Fig. 4. Fractograph of the cured BH-10. The specimen was cured at 200°C for 90 min, and then post-cured at 280°C for 30 min.

In contrast to the distinct two-phase morphology in the cured BH-10, several scattered, globule-like particles coated with a blurring interface can be observed in the cured BC-10 (Fig. 5). This blurring interface comes from the inter-reactions between BPADCy and CPES, through polycyclotrimerizations by the inherent cyanate groups in both components, and indicates good adhesion between particles and matrix. This inter-reaction creates the inter-facial zone, which was fractured under stress and generated the blurring interface. To further demonstrate the inclusion of CPES chains in the BPADCy-rich domain, the cured BC-10 sample was surveyed by TEM. The resulting TEM in Fig. 6 shows that, except in the interfacial region, the dark areas are scattered in the interior of the bright particle domain. The dark area is rich in CPES since the inherent $-SO_2-$ linkages of CPES can be selectively attacked by the staining agent, RuO_4. The bright area is therefore the polycyanurate phase derived from BPADCy. Suggestively, the inclusion of CPES in the BPADCy-rich particles is responsible for the high-temperature T_g reduction observed in Fig. 2.

The catalyst system caused a major morphological change in the cured product. With the inclusion of the 1 wt% catalyst, the cured BH-10C1 loses the distinct two-phase morphology as BH-10 has. Fig. 7 shows that the cured BH-10C1 possesses a similar picture as the cured BC-10, with the scattered particles coated with a layer of blurring interface. Nevertheless, the particle sizes seem to be more heterogeneously distributed when compared with the cured BC-10. The existence of an interface in the cured BH-10C1 may be attributed to the new inter-reaction between the hydroxyl termini in HPES and the cyanate group in BPADCy promoted by the catalyst system. This proposal was supported by a IR absorption at 1650 cm^{-1}, characteristic of the iminocarbonate (–O–C(=NH)–O) bond [22,23] formed through nucleophilic addition of the –OH group in HPES to the –OC≡N group in BPADCy, found for the cured BH-10C1.

All samples discussed above possess a morphology of particle phase dispersed in the matrix phase, however, different morphologies resulted once we increased the incorporated thermoplastic HPES (or CPES) content to 50 wt%. A co-continuous interconnected structure for the cure BC-50 is shown in Fig. 8. This interconnected structure was possibly generated through a spinodal decomposition phase-separation process during the cure of BC-50 and a conclusion had been separated studied by real-time optical microscopy and TEM in our laboratory [15]. The same interconnected structure was observed for the cured BH-50.

Qualitative optical photographs taken for the cured BH-50 were selected and given in 9a–d to illustrate general features of the formation and propagation of various deformation zones after sample immersion in methylene chloride for different time periods. Fig. 9a shows that deformation zone 1 was initiated from the tip of the pre-existing crack

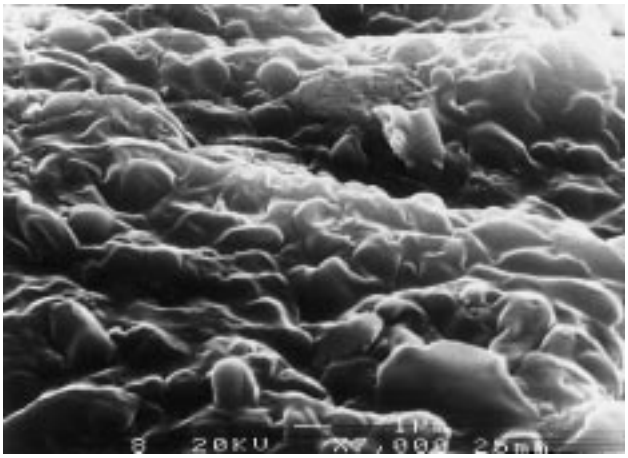

Fig. 5. Fractograph of the cured BC-10. The specimen was cured at 200°C for 90 min, and then post-cured at 280°C for 30 min.

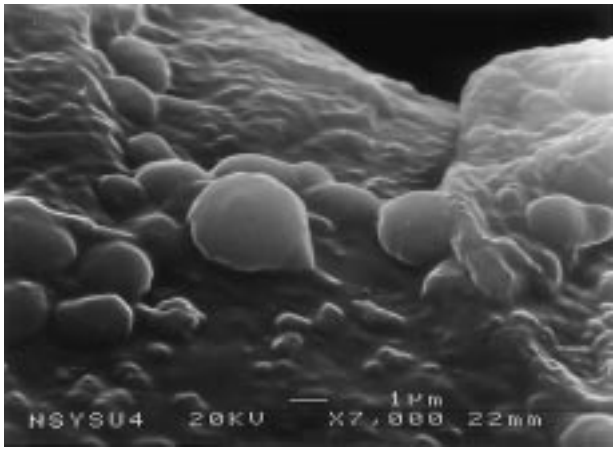

Fig. 7. Fractograph of the cured BH-10C1. The specimen was cured at 200°C for 90 min, and then post-cured at 280°C for 30 min.

while zones 2 and 3 were initiated from other flaws (dust particles or scratches). As propagation proceeded, deformation zone 1 met zone 2 to form a closed loop and zone 3 stopped at the free surface of the pre-existing crack (Fig. 9b). At a later stage, more new zones (such as zone 4 in Fig. 9c and zones 5 and 6 in Fig. 9d) formed and propagated until they finally terminated at the edge of the pre-existing crack. To make sure that all deformation zones propagated steadily, deformation zone lengths of different origins were measured at certain time periods. Fig 10a and b show the length of a number of deformation zones length as a function of immersion time for BH-50 and BC-50, respectively. Clearly, the zones were growing at a constant speed for each sample; different zones initiated at different times but they all grew with the same velocity. The zone growth rate was measured for other samples listed in Table 1. In all cases, the zones grew at the constant speed.

As indicated above, all deformation zones either formed loops with other zones or terminated at a free surface. This process can be schematically explained by Fig. 11. The stress field around the tip of the deformation zone can be illustrated by the continuous stress lines. The stress field in front of the tip of the deformation zone will be compressed once the zone is approaching a free surface or another propagating zone. To retain the continuity, stress lines between the propagating zone and free surface (or other approaching zones) are denser as compared to the rest of the areas. In this manner, stress concentration is generated in certain regions. Consequently, the propagation of the deformation zone will be guided by the stress concentration field, and, of course, toward the direction of the free surface (or other approaching zones). Strain energy was completely released at the free surface (or other approaching zones) and propagation of the deformation zone stopped.

The deformation zone length after immersion in methylene chloride for 1 min was taken as the value of flaw size (a), and fracture toughness (G) thus evaluated were summarized in Table 2. Here, stress (σ) and elastic modulus (E) were calculated from the rule of mixture based on the known values of the pure components, HPES [20] and the cured BPADCy [21]. In addition, σ and E values of HPES

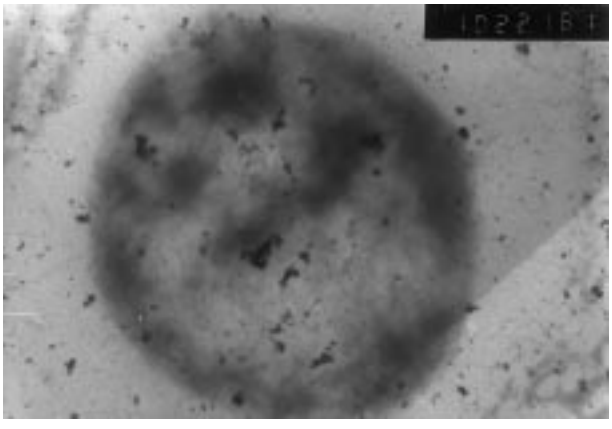

Fig. 6. TEM images of the cured BC-10.

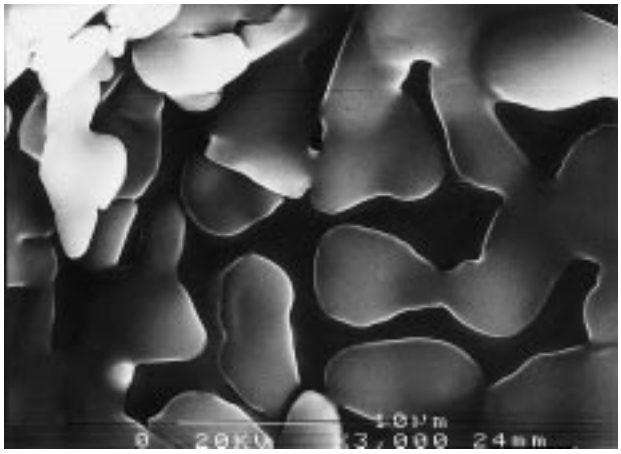

Fig. 8. The fractograph of the cured BC-50. The specimen was cured at 200°C for 90 min, post-cured at 280°C for 30 min, polished and then extracted with methylene chloride for 24 h.

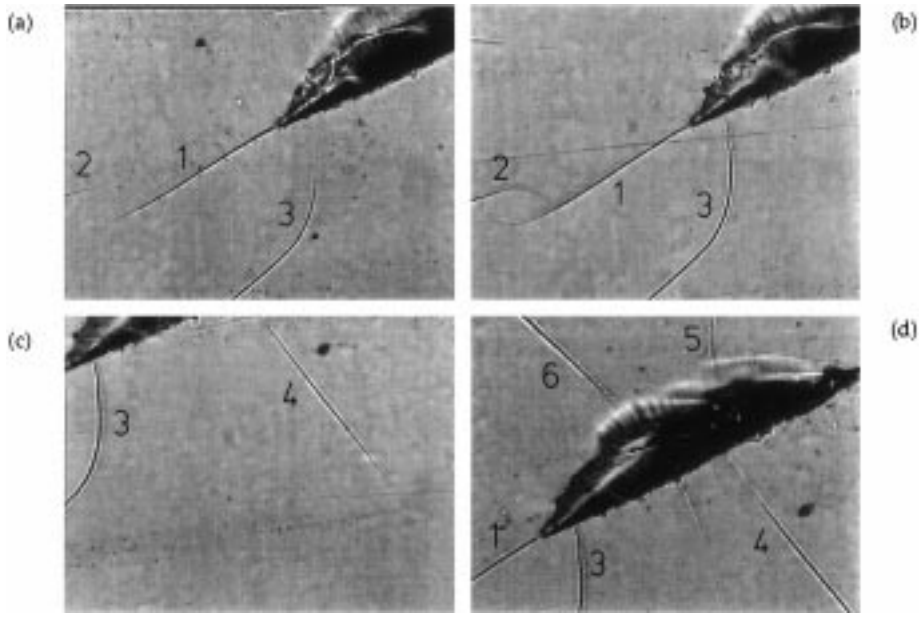

Fig. 9. Propagation of the deformation zone under optical inspection. (a) Initiation of the deformation zone at the edge of the pre-existing crack after film immersion for 3 min. (b) Zone termination by loop-forming after film immersion for 5 min. (c) Zone termination at a free surface after film immersion for 5 min. (d) Formations of various terminated zones after film immersion for 20 min.

were used to replace those for the cured CPES due to the limited amount of CPES samples available for the mechanical study. This may result in an inaccurate G value for the cured BC system; nevertheless, relative magnitude of G values should hold for all samples.

As suggested in Table 2, the cured BPADCy possesses the lowest fracture toughness among all samples, a result correlated with the smooth fracture surface shown in Fig. 3. The cured BH-10, with the toughening effect of the second HPES component, has its G value ($= 33.5$ J/m^2) higher than the cured BPADCy ($= 26.6$ J/m^2). However, the increase of the G value is limited since only small amounts of thermoplastic HPES was used in this sample BH-10, and the resulting fracture surface in Fig. 4 suggests the weak interfacial adhesion between the HPES-rich particle and the polycyanurate matrix. The increasing content of the second phase reasonably increases the surface area between particles and matrix; and this resulted in higher fracture energy. The greater toughness increment of BH-50 (or BC-50) in comparison to BH-10 (or BC-10) can be therefore expected; however, the contribution from the morphological difference should not be negligible. As suggested from the SEM fractographs above, the cured BH-50 (or BC-50) possesses an interconnected structure, in contrast to the dispersed particles observed in the cured BH-10 (or BC-10). In considering the contact surface areas between the two phases, more energy is supposedly required to unlock the interconnected structure (i.e. the cured BH-50 and BC-50) as compared to the dispersed particle cases (i.e. the cured BH-10 and BC-10).

In case of CPES-toughened polycyanurate, an interfacial zone formed between the dispersed particles and matrix. The resulting morphology of the cured BC-10 is therefore distinct from the discrete particle structure in the cured BH-10. The presence of the interfacial zone increases the interfacial adhesion and the toughness of the CPES-toughened polycyanurates (i.e. the cured BC-10 and BC-50). Here, the increment of the G value from the cured BH-50 to BC-50 is more drastic as compared to that from the cured BH-10 to BC-10. Suggestively, the large interfacial area in the interconnected structure of the cured BH-50 would contribute to the greater increment of the fracture toughness if an interfacial zone was generated as in the cured BH-50C1, a situation cannot be met by the cured BH-10 system since only limited interfacial areas are involved here. The interfacial zone also can be created once cure of BH-10 proceeding with addition of the 1 wt% of the catalyst system. Therefore, the cured BH-10C1 has higher fracture toughness as compared to the cured BH-10; also, the cured BH-50C1 is tougher than the cured BH-50. Finally, we noticed that both the cured BC-50 and BH-50C1 have the same calculated G value. Here, the G value of the cured BC-50 may be underestimated because that σ value of HPES, instead of the cured CPES, was used for the calculation. Nevertheless, the comparable magnitude of the resolved toughness for the cured BC-50 and BH-50C1 may indicate that both samples possess a similar interconnected structure with a layer of interfacial zone between the poly(ether sulfone) and the polycyanurate phases.

4. Conclusion

Fracture toughness of the poly(ether sulfone)-blended

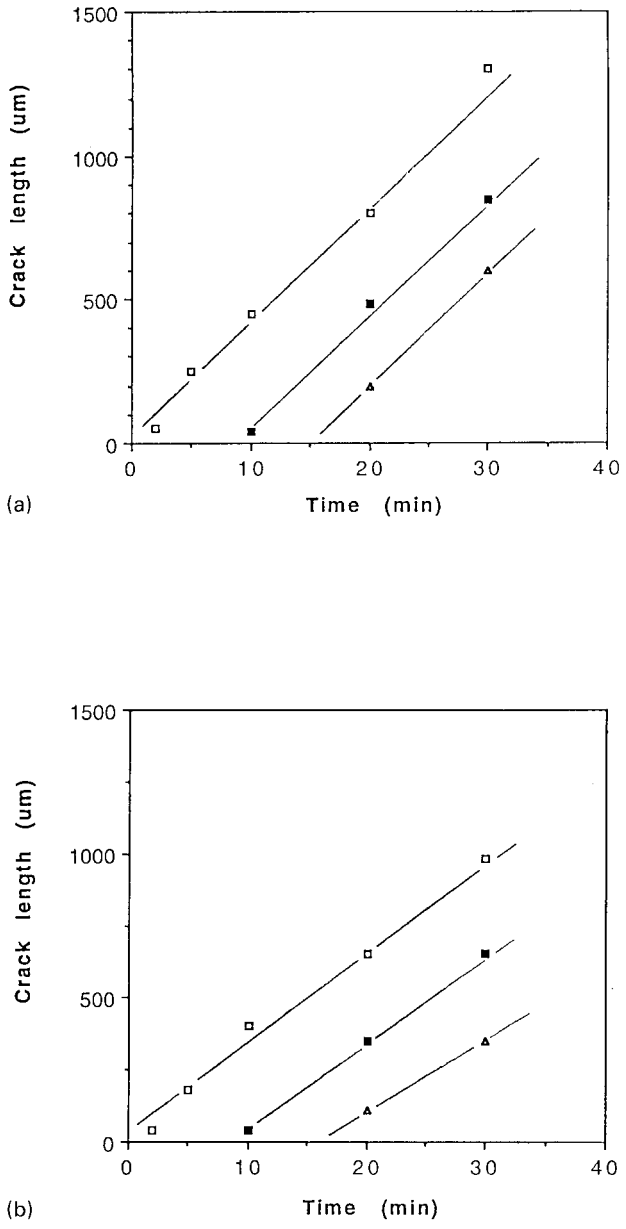

Fig. 10. (a) Length of the deformation zone versus time for the cured BH-50. The slope is 42.6. (b) Length of the deformation zone versus time for the cured BC-50. The slope is 32.4.

polycyanurates was strongly correlated with the corresponding morphology, and the results for all samples were listed in Table 2. With increasing content of the HPES (or CPES) component, the corresponding polycyanurates gained their toughness. With the same thermoplastic content, CPES-toughened polycyanurates possess higher G values as compared to HPES-toughed cases due to the generation of the interfacial zone in the cured BC systems. Similarly, the interfacial zone can also be created by the application of the catalyst in the curing stage, and this will subsequently increase the fracture toughness of the resulting products.

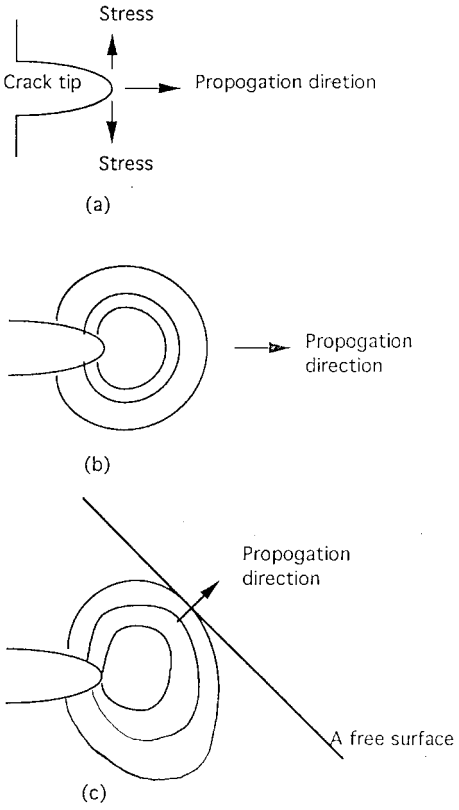

Fig. 11. Mechanism for the propagation of the deformation zone. (a) Stress at the crack tip. (b) Stress field around the crack tip. (c) Variation of the propagation direction due to the compressed stress field.

Table 2
Fracture toughness of different poly(ether sulfone)-reinforced polycyanurate

Sample	σ[a] (Mpa)	a[b] (μm)	E[c] (Gpa)	G[d] (J/m^2)
Cured BPADCy	82.7[e]	4	3.24[e]	26.6
HPES	75[f]	–	2.4[f]	–
Cured BH-10	81.97	5	3.15	33.5
Cure BH-50	78.85	20	2.82	138.5
Cured BC-10	81.98	12	3.16	80.3
Cured BC-50	78.89	60	2.82	416.0
Cured BH-10C1	81.97	10	3.15	67.0
Cured BH-50C1	78.85	60	2.82	415.6

[a] σ is calculated from rule of mixture, $\sigma = \sigma_1 v_1 + \sigma_2 v_2$; where the subscript 1 represents the cured BPADCy and 2 stands for the second poly(ether sulfone) component. The volume fraction of component i, v_i, was calculated from the density value obtained from density gradient method (cf. Section 2).

[b] Flaw size after immersion in methylene chloride for 1 min.

[c] E is evaluated from rule of mixture, $E = E_1 v_1 + E_2 v_2$; where 1 represents the cured BPADCy and 2 stands for the second poly(ehter sulfone) component.

[d] Fracture toughness (G) was calculated from $G = \pi\sigma^2/E$.

[e] Value was taken from Ref. [20].

[f] Value was taken from Ref. [21].

Acknowledgements

We appreciate the financial support of the National Science Council, R.O.C., under contract no. NSC-87-2216-E-110-003.

References

[1] Bucknall CB. Toughened plastics, London: Applied Science, 1977.
[2] Rowe EH, Siebert AR, Draje RS. Mod Plast 1970;47:110.
[3] Sultan JN, McGarry FJ. Polym Engng Sci 1973;13:29.
[4] Riew CK, Rowe EM, Siebert AR. In: Deanin RD, Grugnola AH, editors. Toughness and brittleness of plastics, Advances in Chemistry Series, 154. Washington, DC: American Chemical Society, 1976. p. 326.
[5] McGarry AC. Polymer 1974;15:675.
[6] Manzione LT, Gillham JK, McPherson CA. J Appl Polym Sci 1981;26:889.
[7] Manzione LT, Gillham JK, McPherson CA. J Appl Polym Sci 1981;26:907.
[8] Fang T, Shimp DA. Prog Polym Sci 1995;20:61.
[9] Ayano S, Proc ACS. Polym Mater Sci Engng 1986;54:107.
[10] Woo EM, Fukao B, Seferis JC. Proc. 3rd Tech. Conf. Amer. Soc. Compos. Seattle, 1988. p. 192.
[11] Feldman JA, Huang S. In: Dickie RA, Labana SS, Bauer RS, editors. Crosslinked polymer, ACS Symposium Series, 367. Washington, DC: American Chemical Society, 1988. p. 245.
[12] Cao ZQ, Mechin F, Pauscault JP. Polym Int 1994;34:41.
[13] Woo EM, Shimp DA, Serferis JC. Polymer 1994;35:1658.
[14] Woo EM, Su CC, Kuo JF, Serferis JC. Macromolecules 1994;27:5291.
[15] Chang JY. PhD thesis. National Sun Yat-Sen University, Taiwan, ROC, 1998.
[16] Brown HR, Yang ACM. J Mater Sci 1990;25:2866.
[17] Reed-Hill RE, Abbaschian AR. Physical metallurgy principles, Boston, MA: PWS-KENT Publishing, 1992.
[18] Johnson RN, Farnham AG, Clendinning RA, Hale WF, Merriam CN. J Polym Sci: Part A-1 1967;5:2375.
[19] Chang JY, Hong JL. Macromol Chem Phys 1995;196:3753.
[20] Mark HF, Kroschwitz ZI. Encyclopedia of polymer science and engineering, New York: Wiley, 1988.
[21] Shimp DA. Polym Mater Sci Engng 1986;54:107.
[22] Kohn K, Langer R. Biomaterials 1986;7:176.
[23] Grigat E, Putter R. Chem Ber 1964;97:3022.